Plasmonics (2024) 19:2119–2128
https://doi.org/10.1007/s11468-023-02125-z

RESEARCH

SERS Sensor for Cu^{2+} Detection Based on Etching Reactions

Xiaoyu Du[1] · Na Guo[1] · Guangda Xu[2] · Lixin Xia[1]

Received: 10 October 2023 / Accepted: 14 November 2023 / Published online: 6 December 2023

Abstract
The presence of copper ions (Cu^{2+}) in excessive amounts can pose significant health risks. Therefore, the development of a rapid and highly sensitive technique for detecting even trace quantities of Cu^{2+} is of paramount importance. The proposed detection approach leverages the core-shell design of Au@Ag NPs functioning as the sensing substrate. The substrates were coupled with Raman probe molecules, namely, 4-mercaptobenzoic acid (4-MBA) and iodine ions (I^-), resulting in the formation of the Au@Ag NPs-4-MBA-I^- detection system. In this system, interactions between Cu^{2+} and I^- took place, leading to the generation of I_2, which in turn initiated the etching process of the Ag shell layer. Consequently, the thickness of the Ag shell decreased gradually. This reduction in the shell layer impaired the surface-enhanced Raman scattering (SERS) enhancement effect, causing a gradual decrease in the Raman signal intensity at 1586 cm^{-1} which was attributed to the characteristic peak of 4-MBA. Notably, a linear correlation existed between the thickness of the Ag shell and the intensity of the Raman signal. The proposed method for Cu^{2+} detection exhibits robust resistance to interference and high reproducibility under optimal SERS testing conditions. It boasted a wide linear detection range from 10^{-9} to 10^{-4} M and achieves a low detection limit (LOD) of 1.108 10^{-9} M. Moreover, this sensor was environmentally friendly, offered rapid recognition capabilities, and incurred minimal detection costs. Its versatility extended to diverse water systems, making it suitable for detecting Cu^{2+} not only in tap water but also in various other water sources.

Keywords Cu^{2+} · SERS · Sensor · Etching reaction

Introduction

Heavy metals are natural components in the Earth's crust, released into the environment as a result of human activities, and resistant to natural degradation processes. The consequences of even minute quantities of heavy metals (1 ppm) on human well-being cannot be ignored [1–4]. Among these heavy metals, copper ions (Cu^{2+}) exhibit both beneficial and detrimental impacts on human physiology. On one hand, they contribute significantly to vital metabolic functions; on the other hand, an excessive influx of Cu^{2+} can lead to various diseases, including anemia and Alzheimer's disease [5, 6]. Notably, the typical concentration of naturally occurring Cu^{2+} in freshwater ranges from 0.20 to 30 ng/mL [7, 8]. Different countries establish distinct regulations governing the permissible Cu^{2+} levels in water, highlighting the importance placed on maintaining appropriate Cu^{2+} concentrations. Consequently, the recognition and precise detection of Cu^{2+} in water sources have become increasingly important. Current methodologies for Cu^{2+} detection encompass techniques such as atomic absorption spectroscopy (AAS) [9], atomic emission spectrometry (AES) [10], and inductively coupled plasma mass spectrometry (ICP-MS) [11]. However, these conventional methods entail intricate sample preparation and instrument operation, rendering them unsuitable for rapid sample analyses.

In recent years, SERS technology has garnered considerable attention for its ability to detect Cu^{2+} due to its high sensitivity, low detection limit, and reduced time constraints. A notable advancement was made by Liu et al., who introduced a novel and stable SERS sensor for Cu^{2+} detection [12]. Their approach entails utilizing Ag NPs coated with inositol hexaphosphate (IP6) as the SERS substrate. The

✉ Guangda Xu
xuguangdalnu@163.com

✉ Lixin Xia
lixinxia@lnu.edu.cn

1 College of Chemistry, Liaoning University, Shenyang 110036, China

2 School of Pharmacy, Shenyang Pharmaceutical University, Shenyang 110016, China

substrate was further modified with L-cysteine, and Cu^{2+} is quantitatively identified using R6G as the SERS probe. Similarly, Guo et al. reported a method for Cu^{2+} detection using Ag-Au satellite structures. Here, Ag NPs were functionalized with 4-mercaptobenzoic acid (4-MBA), while Au NPs were modified with 4-mercapto pyridine (4-Mpy) [5]. After the addition of Cu^{2+}, the carboxyl groups in 4-MBA and the N atoms in pyridine formed coordination bonds with Cu^{2+}, inducing the aggregation of both Ag and Au NPs. This aggregation resulted in enhanced SERS signal peaks characteristic of 4-MBA and 4-Mpy. Despite these advancements in utilizing SERS for Cu^{2+} detection, they still face problems such as complex probe molecules and substrates. Therefore, there is an urgent need for a simpler approach to Cu^{2+} detection using simple SERS substrates and probe molecules. Although these methods have achieved the detection of Cu^{2+} through SERS technology, they still face problems such as complex probe molecules and complex substrates.

In this work, we introduced a SERS sensor characterized by its simple sample preparation, high sensitivity, and rapid Cu^{2+} detection capabilities. The SERS substrate consisted of 4-MBA functionalized onto a core-shell structure of Au@Ag NPs. By introducing an iodine ion (I^-) solution, a dynamic system was established capable of Cu^{2+} detection. Upon the addition of Cu^{2+}, the reaction between I^- and Cu^{2+} initiated the etching of the Ag shell layer. This etching led to a reduction in the hot spot region of the system, subsequently attenuating the enhancement effect on Raman probe molecules. "Hot spots" for SERS were defined as the area where great EM enhancement existed [13, 14]. Consequently, the SERS signal intensity associated with 4-MBA at 1586 cm^{-1} decreased. A robust linear correlation was observed between the change in SERS signal intensity at 1586 cm^{-1} and the logarithm of Cu^{2+} concentration within the range of 10^{-9} to 10^{-4} M. Notably, the LOD reached a low value of 1.108×10^{-9} M. The applicability of this methodology extended successfully to the analysis of Cu^{2+} within tap water samples, thereby introducing a new approach to detecting trace amounts of Cu^{2+} in real-world environments. The schematic representation of this quantitative detection approach is illustrated in Fig. 1.

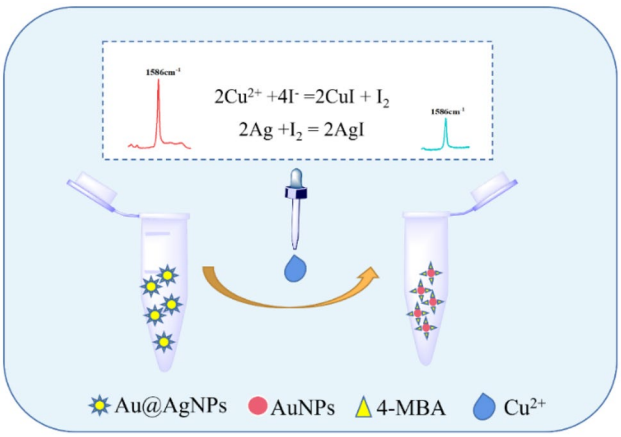

Fig. 1 Schematic illustration of Cu^{2+} sensor

Experimental Section

Materials

All reagents and solvents used were of analytical grade, and the chemicals were used with no further purification. The materials encompassed 4-MBA, sodium citrate, ascorbic acid (AA), KI, $HAuCl_4 \cdot 3H_2O$, $AgNO_3$, $Cu(NO_3)_2$, $HgCl_2$, $Co(NO_3)_2$, $Mn(NO_3)_2$, $Ni(NO_3)_2$, $Zn(NO_3)_2$, $Fe(NO_3)_2$, $Fe(NO_3)_3$, and $Cd(NO_3)_2$, and ethanol was purchased from Energy Chemical Co., Ltd. (China). Deionized water was utilized in the preparation of the experimental solutions.

Instrumentation

The characterization of Ag NPs and Au@Ag NPs involved the utilization of a JEM-2100 ultra-high-resolution transmission electron microscope (JEOL, Japan) to determine their geometry and size. Additionally, the size of Ag NPs and Au@Ag NPs was determined using a nanoparticle zeta potential analyzer (DLS). Ultraviolet-visible (UV-vis) absorption spectra were recorded using a PerkinElmer Lambda 35 spectrophotometer (326 nm; Norwalk, CT, USA). Elemental composition was established using K-Alpha X-ray photoelectron spectroscopy (XPS), while ion content was quantified using an inductively coupled plasma mass spectrometer (ICP-MS). Material composition was determined via X-ray diffractometer (XRD) analysis. SERS measurements were conducted using a Renishaw inVia reflex confocal microscope (Renishaw, UK). These measurements were facilitated by a He-Ne laser (532 nm, exposure time of 10 s). The laser spot diameter was 1 μm, and a laser power of 50 mW was utilized throughout the experimentation.

Synthesis and Characterization of Au@Ag NPs

The synthesis procedure for Au@Ag NPs is based on existing literature with slight modifications [15]. First, 60 mL of deionized water was combined with 950 μL of a 5 g/L chloroauric acid solution in a reaction vessel; the mixture was subsequently magnetically stirred. The temperature was then increased to 120 ℃ and maintained for 1 min. Following this, 600 μL of an aqueous 1% trisodium citrate solution was rapidly injected into the solution while stirring vigorously; the mixture was left to boil for 5 min. During this process,

the solution changed from colorless to purple-red, signifying the successful formation of Au NPs. The resulting colloidal solution was allowed to cool to room temperature and was subsequently stored at 4 ℃.

In a separate container, 3 mL of the Au NP colloidal solution was sonicated for 10 min. Subsequently, 270 µL of a 10 mM AA solution was added, and the mixture was stirred for 15 min. While maintaining stirring, 150 µL of a 10 mM $AgNO_3$ solution was added dropwise to the mixture, and the mixture was stirred for 20 min. During this reaction, the solution changes from purple-red to orange, indicating the successful formation of Au@Ag NPs. The resulting colloidal solution was stored at 4 ℃ for future use.

Preparation of Cu^{2+} Standard Solution and Samples

First, $Cu(NO_3)_2$ was dissolved in deionized water to yield a 1 mM solution. Subsequently, a range of Cu^{2+} solutions with varying concentrations were prepared by diluting the 1 mM $Cu(NO_3)_2$ solution accordingly. For real water sample analysis, tap water from Shenyang, Liaoning Province, China, was collected. The collected water samples were then filtered through a 0.45-µM filter membrane to remove insoluble particles and impurities.

Cu^{2+} Detection

First, 200 µL of 4-MBA solution, 200 µL of Au@Ag NPs, 200 µL of KI, and 200 µL of either Cu^{2+} solution or various concentrations of spiked water solution were sequentially transferred into a centrifuge tube. After complete sonication and thorough mixing at ambient temperature, SERS detection was carried out. Using a He-Ne laser (532 nm) with a laser power set at 50 mW, the change in SERS intensity at 1586 cm^{-1} corresponding to 4-MBA was selected as the quantification benchmark. Each experimental iteration was conducted in triplicate to ensure robustness and consistency.

Results and Discussion

Characterization of Au@Ag NP SERS Substrate

To gain deeper insights into the dimensions and structure of the substrate and to validate its successful synthesis, we conducted comprehensive characterizations involving TEM, DLS, and UV-vis analyses, as shown in Fig. 2. Initially, we characterized the Au NPs during the substrate synthesis process. As illustrated in Fig. 2A, the TEM image of the Au NPs revealed a spherical morphology, depicting a uniform dispersion and relatively consistent size. From the DLS data in Fig. 2B, it was evident that the size of these Au NPs was approximately 15 nm. Furthermore, Fig. 2C displays the UV absorption spectrum of the Au NPs, wherein the absorption peak was situated at 523 nm, effectively confirming the successful synthesis of a spherical Au core. Subsequently, our focus shifted to the core-shell configuration of the Au@Ag NPs, characterized via TEM, DLS, and UV-vis analyses as shown in Fig. 2D–F. The TEM images substantiated the successful encapsulation of the Ag shell layer around the exterior of the Au NPs, resulting in the formation of Au@Ag NPs. These possess a uniform size, further validated by the DLS measurements indicating an average particle size of approximately 34 nm. Notably, the UV absorption peaks were located at 394 nm and 491 nm, corresponding to the plasmon resonance of the Ag shell and Au core [16]. This multifaceted characterization robustly confirmed the successful synthesis of Au@Ag NPs, thus establishing their viability as detection substrates for subsequent analyses.

To validate the composition of the synthesized substrate as a valuable metal substrate encompassing both Au and Ag, XPS analysis was conducted on both the Au NPs and Au@Ag NPs, as depicted in Fig. 3. As shown in Fig. 3A, the XPS spectrum indicated that the substrate contains gold and silver components. The binding energy of 83.9 eV corresponds to the 4f orbital of Au, specifically Au $4f_{5/2}$, while 87.7 eV corresponds to Au $4f_{7/2}$ in Fig. 3B. The binding energies of the Ag 3d orbital were recorded at 368.2 eV (Ag $3d_{5/2}$) and 374.2 eV (Ag $3d_{3/2}$) in Fig. 3C. These distinctive binding energies derived from the XPS analysis affirm the presence of both Au and Ag components within the synthesized substrate.

Detection and Characterization Mechanism for Cu^{2+}

The presence of sulfhydryl groups within 4-MBA molecules enabled a strong S-Ag bond formation, facilitating the adsorption of 4-MBA onto the surface of Au@Ag NPs. This interaction generated robust SERS signal peaks within the hot spot regions of Au@Ag NPs. Specifically, the SERS signal peaks of 4-MBA were mainly located at 997, 1012, 1077, 1138, 1181, 1586, and 1706 cm^{-1} [17, 18]. Among these, the signal peak at 1586 cm^{-1} exhibited both strength and distinctiveness, making it an ideal candidate for quantitative analysis. Therefore, the peak at 1586 cm^{-1} was selected as the characteristic peak for quantitative analysis. The Cu^{2+} detection mechanism relied on a series of chemical reactions. Since (Cu^{2+}/Cu) [φ^{θ} (Cu^{2+}/ Cu) = 0.3402 V], (Ag^{+}/Ag) [φ^{θ} (Ag^{+}/Ag) = 0.7996 V]. By considering the relationship between electrode potential and the direction of the reaction, it became evident that direct interaction between Cu^{2+} and Au@Ag NPs is unlikely. However, upon the introduction of I^{-} into the system, Cu^{2+} underwent a reaction generating CuI precipitates and I_2. Subsequently, I_2 quantitatively reacted with Ag to produce AgI, inducing a series of reactions: $2Cu^{2+} + 4I^{-} = 2CuI + I_2$, $I_2 + 2Ag = 2AgI$. The occurrence

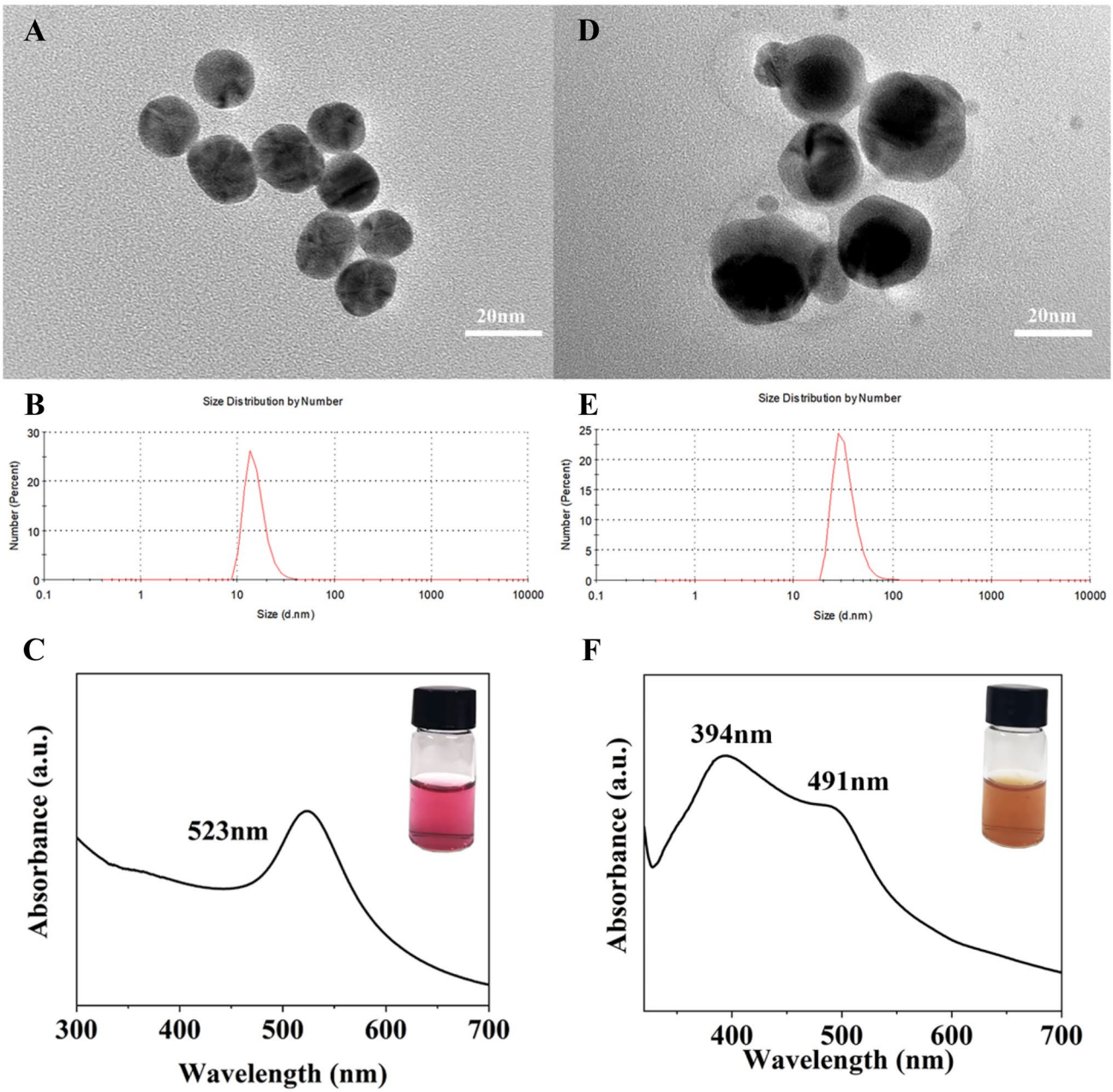

Fig. 2 TEM, DLS, and UV-vis images of Au NPs and Au@Ag NPs

of these reactions led to the etching of the Ag shell layer. As the Ag shell thins, the SERS enhancement effect diminishes, resulting in a reduction of the SERS signal attributed to 4-MBA molecules at 1586 cm^{-1}. Consequently, a linear correlation was established between the concentration of Cu^{2+} and the SERS signal intensity of 4-MBA molecules.

To validate the accuracy of our explanation regarding the Cu^{2+} detection mechanism, we initially conducted a comprehensive analysis of the overall changes occurring during the detection process, utilizing UV-vis and TEM techniques. In Fig. 4A, the UV-vis spectrum displayed noteworthy alterations, upon introduction of I^- and Cu^{2+} into the system, resulting in absorption peaks at 426 nm and 558 nm, respectively, where were related to the SPR absorption of AgI and Au, respectively [19, 20]. Figure 4B displays a TEM image of the etched system, clearly illustrating a significant thinning of the Ag shell layer when compared to the previous image. This tangible transformation provided visual evidence of the etching of the Ag shell layer, thereby confirming the occurrence of the reaction. Furthermore, to further prove the occurrence of the etching reaction during the detection process, we delved into the valence changes

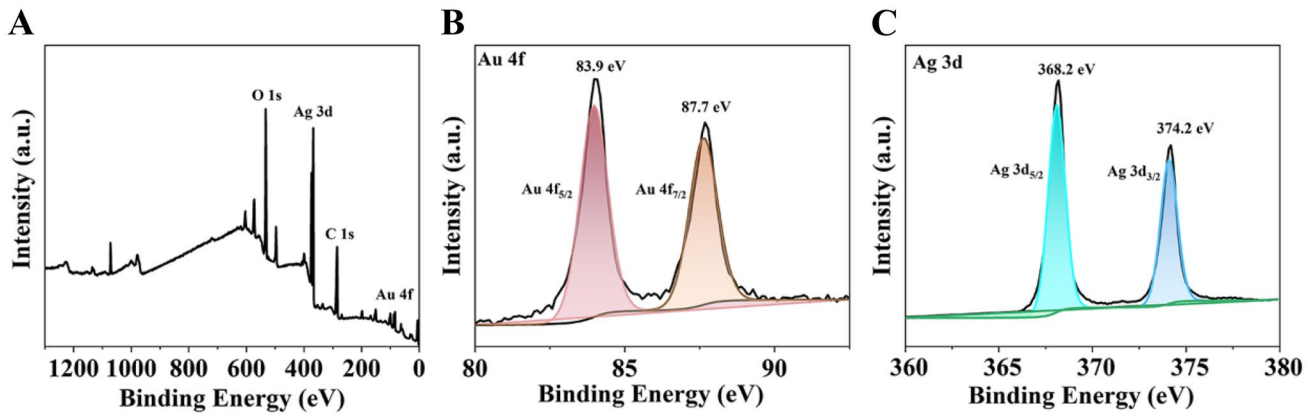

Fig. 3 XPS images of Au@Ag NPs

of elements within the process and analyzed the resultant reaction products. The change in element valence during the reaction was analyzed via XPS characterization. In Fig. 4C, the Ag within the Au@Ag NPs was identified as Ag^0, with its binding energy located at 368.2 eV and 374.2 eV. However, after the addition of I^- and Cu^{2+}, discernible shifts in binding energy were observed, accompanied by the emergence of new spectral peaks at 366.3 eV and 372.6 eV, which were attributed to generated Ag^+ ions. The detection system was further characterized by XRD, as shown in Fig. 4D. It could be observed that the diffraction pattern reveals distinct peaks at 38.2°, 44.5°, 64.6°, and 77.7°, which correspond to the characteristic crystal planes of AgI (110) and (220) and Ag and Au (111) and (200), respectively. This outcome validated the formation of AgI and, by extension, the occurrence of the anticipated etching reactions.

To validate the feasibility of the SERS detection principle, a comprehensive analysis was conducted using SERS technology. Figure 5 shows the SERS signals of the Au@Ag NPs-4-MBA-I^--Cu^{2+} system. From the figure, curve a was the Raman spectrum of Au@Ag NPs, where it was evident that Au@Ag NPs did not exhibit any discernible characteristic peaks. This observation effectively confirmed that the substrate does not induce signal interference during Cu^{2+}

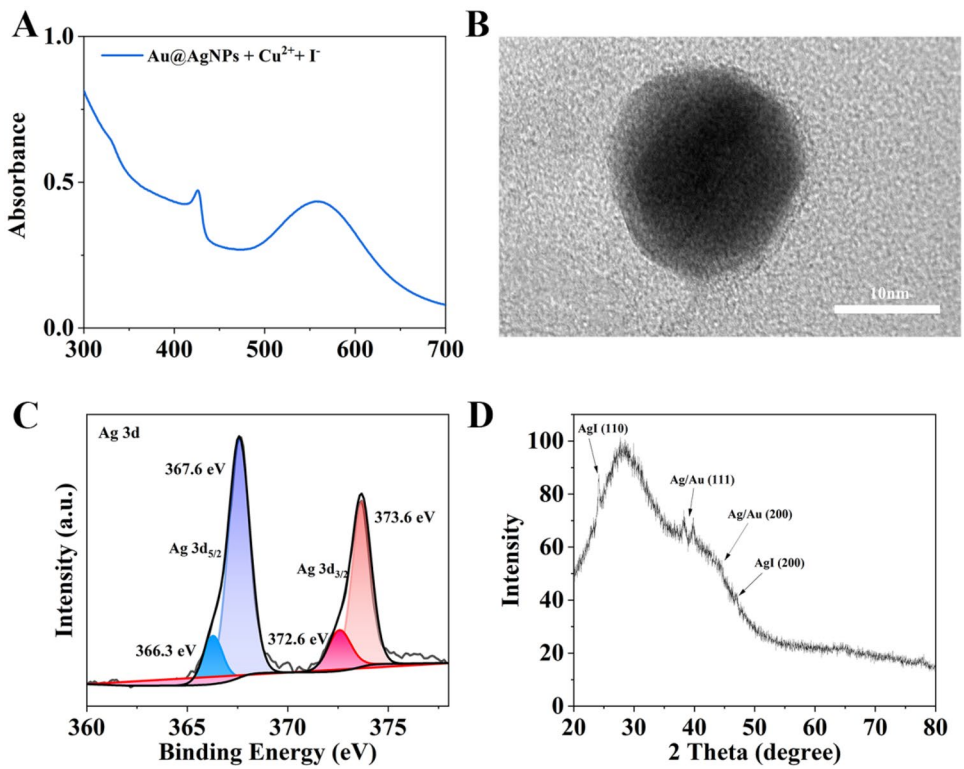

Fig. 4 UV-vis, TEM, XPS, and XRD images of the Au@Ag NP etching reaction

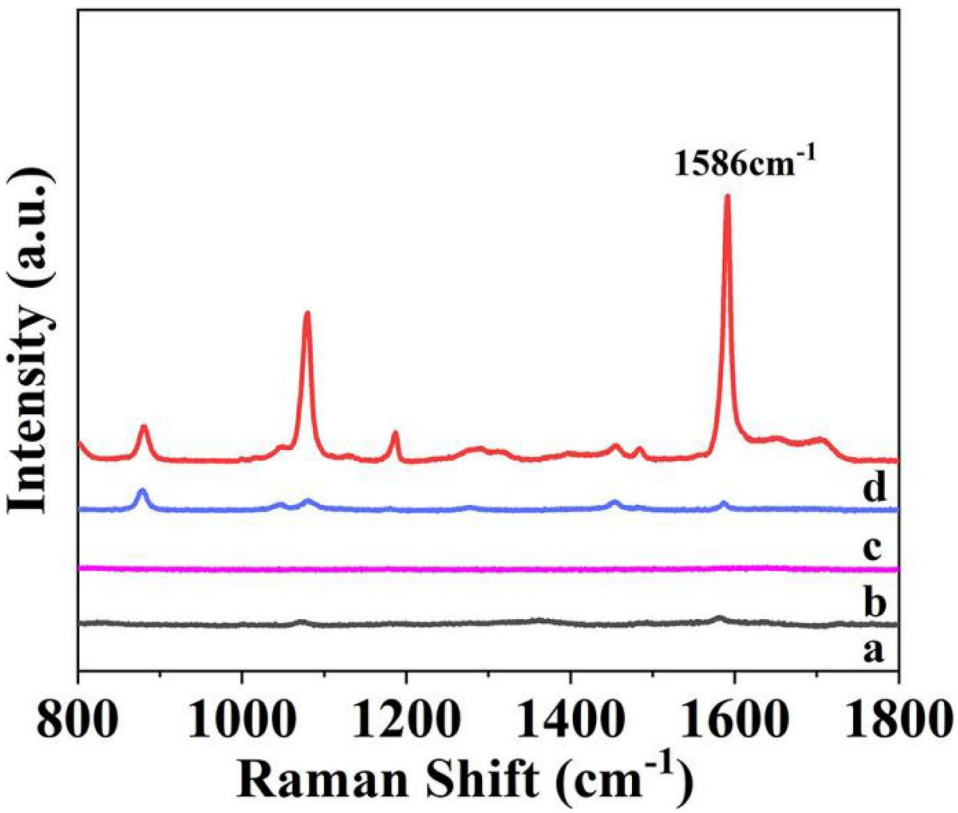

Fig. 5 SERS spectra of (a) Au@Ag NPs, (b) Au@Ag NPs + 10^{-3} M I^-, (c) Au@Ag NPs + 10^{-3} M 4-MBA + 10^{-3} M I^- + 10^{-3} M Cu^{2+}, and (d) Au@Ag NPs + 10^{-3} M 4-MBA

detection. Curve c was the Raman spectrum of the Au@Ag NPs-4-MBA system, indicating an easily analyzed SERS spectrum of 4-MBA in the 800–1800 cm^{-1} range. Notably, a robust SERS characteristic peak at 1586 cm^{-1} emerged, which could be attributed to the stretching vibration mode of the benzene ring within 4-MBA. This particular peak was designated as the representative SERS characteristic peak. Curve b was the SERS spectrum of the Au@Ag NPs-I^- system; it proved that the Au@Ag NPs-I^- system did not coexist. Curve c was the SERS spectrum of the Au@Ag NPs-4-MBA-I^- system following the introduction of 10^{-3} M Cu^{2+}. Notably, a significant decrease was observed in the characteristic peak at 1586 cm^{-1} compared to curve d, which was due to the etching of Au@Ag NPs by the reaction products of I^- and Cu^{2+}. The resultant reaction led to a decrease in the thickness of the Ag shell and a decrease in the "hot spot" region, which weakened the enhancement effect on 4-MBA molecules and led to a sharp decrease in SERS intensity at 1586 cm^{-1}.

Optimization of the Analytical Conditions

To enhance the sensitivity of Cu^{2+} detection, various factors influencing the testing process were optimized. These optimizations involved the concentrations of 4-MBA, Au@Ag NPs, and I^- solution, as well as reaction time.

The concentration of probe molecules significantly impacted the intensity of SERS signals. Elevated concentrations could lead to multi-layer adsorption on the substrate surface, while excessively low concentrations resulted in single-layer unsaturated adsorption. In contrast, an optimal concentration yielded monolayer saturated adsorption, which aligned with the EM enhancement mechanism for maximum SERS signal strength. Figure S1A illustrates that the highest SERS intensity was observed at a concentration of 5×10^{-3} M, indicating of the monolayer saturated adsorption of 4-MBA onto the Au@Ag NP surface. Therefore, 5×10^{-3} M was selected as the optimal concentration for 4-MBA.

The concentration of the substrate affected the size of the "hot spot" region, thereby affecting the robustness of the SERS signal emitted by the Raman probe molecule. If the substrate concentration was too low, the probe molecules would not have enough adsorption sites, resulting in a weak SERS signal. Conversely, an excessively high substrate concentration could induce substrate aggregation, leading to a reduced area accessible for probe molecule adsorption and a reduced SERS signal strength. The concentrations of the previously synthesized Au@Ag NPs were denoted as c. Based on this, Au@Ag NP substrates were derived at concentrations of 2c, c/2, c/3, and c/4 using centrifugation and dilution techniques. These five

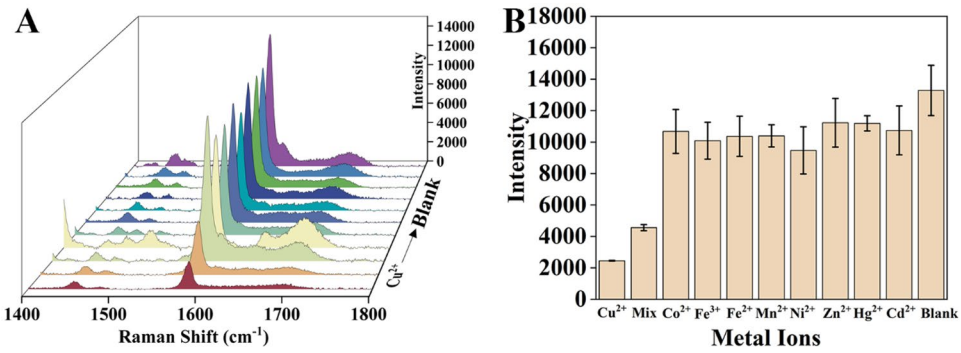

Fig. 6 Selectivity and anti-interference capability of the sensor for Cu^{2+} detection

substrate concentrations were optimized, and the results are shown in Fig. S1B. The SERS signal at 1586 cm^{-1} for 4-MBA exhibited the highest intensity at a concentration of c. Therefore, a substrate concentration of c was selected for subsequent detection.

The detection of Cu^{2+} was carried out via an etching reaction, which was a quantitative process. KI operated as a pivotal reactant, significantly influencing the progression of the etching reaction and subsequently affecting the Cu^{2+} detection results. From Fig. S1C, it could be observed that there were no significant changes in the SERS signal peak intensity at 1586 cm^{-1} under varying KI concentrations, indicating that the concentration of KI had no significant effect on the reaction dynamics. This could be attributed to the substantial disparity between the concentration of Cu^{2+} to be detected and that of KI. Therefore, any KI concentration could be utilized to react with the target Cu^{2+}. For this study, a KI concentration of 10^{-3} M was selected.

The reaction time affected the completeness of a reaction. After the reaction was complete, there would be no significant change in the SERS signal. From Fig. S1D, after 10 min of reaction, the SERS signal tended to stabilize, indicating that the reaction was complete. Therefore, 10 min was selected as the optimal reaction time.

Selectivity for the Au@Ag NP-4MBA-KI Detection System

To validate the selectivity and anti-interference capability of the SERS sensor towards Cu^{2+}, we examined the effects of various metal cations, including Co^{2+}, Fe^{3+}, Fe^{2+}, Mn^{2+}, Ni^{2+}, Zn^{2+}, Hg^{2+}, and Cd^{2+}, as shown in Fig. 6. Notably, the introduction of Cu^{2+} initiated the etching of the Ag shell layer, leading to a reduction in the signal enhancement capability of the SERS substrate, which resulted in a significant decrease in the SERS intensity at 1586 cm^{-1}. Interestingly, the presence of other metal cations did not yield a significant impact on the generation of SERS signals from 4-MBA molecules, indicating that the SERS sensor had strong anti-interference capabilities and selectively detected Cu^{2+}.

Quantitative SERS Detection of Cu^{2+}

To evaluate the sensitivity and potential applicability of the proposed method for quantitative analysis, we conducted measurements using various concentrations of Cu^{2+} standard samples. Under the optimal conditions, our method displayed a linear correlation between Cu^{2+} concentrations and SERS intensity within the range of 10^{-9} to 10^{-4} M with a LOD of 1.108×10^{-9} M. This correlation was well-described by the

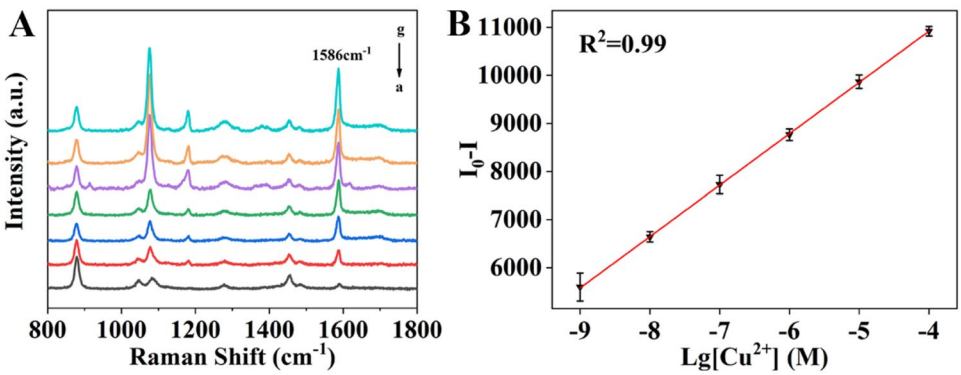

Fig. 7 **A** SERS spectra of Au@Ag NP-4-MBA-I^- system with different concentrations of Cu^{2+} (from a to g are 10^{-4}, 10^{-5}, 10^{-6}, 10^{-7}, 10^{-8}, 10^{-9}, and 0 M) and **B** plot of corresponding intensity

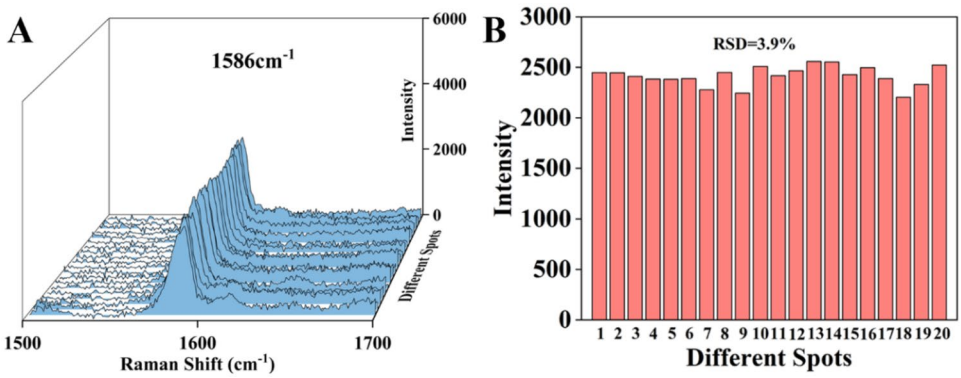

Fig. 8 **A** SERS intensity at 1586 cm^{-1} measured from 20 random positions and **B** series of SERS spectra of a 10^{-5} M Cu^{2+} solution from 20 random positions

Table 1 Cu^{2+} detection in tap water samples via the SERS and ICP-MS methods

Samples	Spiked amount (nM)	SERS amount (nM)	SERS recovery (%)	RSD% ($n=5$)	Spiked amount (nM)	ICP-MS amount (nM)	ICP-MS recovery (%)
Tap water	0	Not detected	–	–	0	Not detected	–
	0.1	0.11	110	1.12	0.1	0.09	111.1
	1	1.07	107	0.114	1	1.03	97.09
	10	9.99	99	0.132	10	9.82	101.8

equation $Y = 1047.72072X + 15{,}026.12795$ ($R^2 = 0.999$), as depicted in Fig. 7, which illustrated the connection between SERS signal intensity and Cu^{2+} concentration. To provide context, the experimental results of other methods for measuring Cu^{2+} are listed in Table S1, indicating the simplicity of our method.

Reproducibility of Cu^{2+} Detection

To evaluate the reproducibility, a total of 20 data points were collected through random sampling under the established optimal experimental conditions. The outcome of this assessment is shown in Fig. 8. It was worth noting that the SERS intensity at 1586 cm^{-1} is relatively uniform across the data points, and the relative standard deviation of the 20 data sets remains below 5%, which served to validate the reproducibility of the proposed SERS sensor methodology.

Analysis of Cu^{2+} in Tap Water Samples

To demonstrate the practicality of the developed SERS method, we utilized it to quantify Cu^{2+} concentrations present in tap water under the optimized conditions using the standard addition method. Different concentrations of Cu^{2+} were tested three times, and the results are shown in Fig. S2. Furthermore, we conducted a comprehensive comparative assessment involving the developed SERS method and the conventional ICP-MS method; the pertinent data are shown in Table 1. Remarkably, the Cu^{2+} concentrations detected by the SERS sensor are consistent with those measured using the ICP-MS method. The recovery rates for Cu^{2+} ranged from 93.68 to 100.91%. This highlighted the reliability and practical applicability of our method for the accurate detection of Cu^{2+} levels in tap water.

Conclusion

In summary, we introduced a novel SERS sensor based on an etching reaction mechanism for the detection of Cu^{2+}. The SERS detection substrate, Au@Ag NPs, coupled with the SERS probe molecule 4-MBA, played a pivotal role in this method. After adding I^- to the system, a specific reaction between I^- and Cu^{2+} was initiated, generating iodine species capable of etching the Ag shell. The extent of Ag shell etching varied with the quantity of iodine produced, subsequently affecting the enhancement effect of 4-MBA molecules varies and influencing the intensity of SERS signals generated at 1586 cm^{-1}. Based on the experimental results, a robust linear correlation between the logarithm of Cu^{2+} concentration and I_0-I was evident within the concentration range of 10^{-9} to 10^{-8} M, with a low LOD of 1.108×10^{-9} M. Moreover, the practical applicability of this method extended to the detection of Cu^{2+} in real water samples, effectively presenting a new method for Cu^{2+} detection. Whether the substrate and Raman probe molecules fail after the test solution has been left for some time, whether the test data are

still accurate, whether the test method is time-sensitive, and the effect of different thicknesses of the silver shell layer and different particle sizes of the gold nuclei on the reaction need to be investigated subsequently.

Supplementary Information The online version contains supplementary material available at https://doi.org/10.1007/s11468-023-02125-z.

Author Contribution All authors contributed to the study conception and design. Material preparation, data collection, and analysis were performed by X. D., N. G., G. X., and L. X. The first draft of the manuscript was written by X. D. and N. G., and all authors commented on previous versions of the manuscript. All authors read and approved the final manuscript.

Funding This work was supported by National Natural Science Foundation of China (21671089), the Liaoning Revitalization Talents Program of China (XLYC2002097), the Scientific Research Fund of Liaoning Provincial Education Department (L2020002), the Liaoning Provincial Natural Science Foundation (2020-YKLH-22), the Key Projects of Liaoning Provincial Education Department (JYTZD2023001), and the Yingkou Revitalization Talents Program of Liaoning.

Availability of Data and Material The data that support the findings of this study are available on request from the corresponding author.

Declarations

Ethics Approval This research does not include human or animal subjects.

Competing Interests The authors declare no competing interests.

References

1. Amit P, Ajay K, Zhong H et al (2018) Adverse effect of heavy metals (As, Pb, Hg, and Cr) on health and their bioremediation strategies: a review. Int Microbiol 21:97–106. https://doi.org/10.1007/s10123-018-0012-3
2. Abdu N, Abdullahi A, Abdulkadir A et al (2017) Heavy metals and soil microbes. Environ Chem Lett 15:65–84. https://doi.org/10.1007/s10311-016-0587-x
3. Cai C, Zhao M, Yu Z et al (2019) Utilization of nanomaterials for in-situ remediation of heavy metal(loid) contaminated sediments: a review. Sci Total Environ 662:205–217. https://doi.org/10.1016/j.scitotenv.2019.01.180
4. Ashraf S, Ali Q, Zahir ZA et al (2019) Phytoremediation: environmentally sustainable way for reclamation of heavy metal polluted soils. Ecotox Environ Safe 174:714–727. https://doi.org/10.1016/j.ecoenv.2019.02.068
5. Guo YY, Li D, Zheng SP et al (2020) Utilizing Ag–Au core-satellite structures for colorimetric and surface-enhanced Raman scattering dual-sensing of Cu (II). Biosens Bioelectron 159:112192. https://doi.org/10.1016/j.bios.2020.112192
6. Uauy R, Olivares M, Gonzalez M et al (1998) Essentiality of copper in humans. Am J of Clin Nutr 67:S952–S959. https://doi.org/10.1093/ajcn/67.5.952S
7. Ye YJ, Lv MX, Zhang XY et al (2015) Colorimetric determination of copper(II) ions using gold nanoparticles as a probe. RSC Adv 5:102311–102317. https://doi.org/10.1039/C5RA20381C
8. Wu Q, Wang XJ, Rasaki SA et al (2018) Yellow-emitting carbon-dots-impregnated carboxy methyl cellulose/poly-vinyl-alcohol and chitosan: stable, freestanding, enhanced-quenching Cu^{2+}-ions sensor. J Mater Chem C 6:4508–4515. https://doi.org/10.1039/C8TC00660A
9. Tatiane MO, Jayme AP, Maria LF et al (2017) Direct determination of Pb in raw milk by graphite furnace atomic absorption spectrometry (GF AAS) with electrothermal atomization sampling from slurries. Food Chem 229:721–725. https://doi.org/10.1016/j.foodchem.2017.02.143
10. Ozbek N, Akman S (2016) Method development for the determination of calcium, copper, magnesium, manganese, iron, potassium, phosphorus and zinc in different types of breads by microwave induced plasma-atomic emission spectrometry. Food Chem 200:245–248. https://doi.org/10.1016/j.foodchem.2016.01.043
11. Khan N, Jeong IS, Hwang IM et al (2014) Analysis of minor and trace elements in milk and yogurts by inductively coupled plasma-mass spectrometry (ICP-MS). Food Chem 147:220–224. https://doi.org/10.1016/j.foodchem.2013.09.147
12. Liu Y, Wu LP, Guo XY et al (2019) Rapid and selective detection of trace Cu^{2+} by accumulation- reaction-based Raman spectroscopy. Sensor Actuat B Chem 283:278–283. https://doi.org/10.1016/j.snb.2018.12.043
13. Tang HB, Zhu CH, Meng GW et al (2018) Review—Surface-enhanced Raman scattering sensors for food safety and environmental monitoring. J Electrochem Soc 165:3098–3118. https://iopscience.iop.org/article/10.1149/2.0161808jes
14. Chen S, Meng LY, Shan HY et al (2016) How to light special hot spots in multiparticle–film configurations. ACS Nano 10:581–587. https://doi.org/10.1021/acsnano.5b05605
15. Zeng JB, Cao YY, Chen JJ et al (2014) Au@Ag core/shell nanoparticles as colorimetric probes for cyanide sensing. Nanoscale 6:9939–9943. https://doi.org/10.1039/C4NR02560A
16. Wang KQ, Sun DW, Pu HB et al (2019) Stable, flexible, and high-performance SERS chip enabled by a ternary film-packaged plasmonic nanoparticle array. ACS Appl Mater Interfaces 11:29177–29186. https://doi.org/10.1021/acsami.9b09746
17. Li YJ, Shi QR, Zhang PN et al (2018) Empirical structural design of core@shell Au@Ag nanoparticles for SERS applications. J Mater Chem C 4:6649–6656. https://doi.org/10.1039/C6TC01499B
18. Zhang XY, Han DL, Pang ZY et al (2018) Charge transfer in an ordered Ag/Cu_2S/4-MBA system based on surface-enhanced Raman scattering. J Phys Chem C 122:5599–5605. https://doi.org/10.1021/acs.jpcc.8b00701
19. Mahnaz EK, Colby F (2000) Optical properties of gold−silver iodide nanoparticle pair structures. J Phys Chem B 104:4031–4037. https://doi.org/10.1021/jp992632h
20. Zeng JB, Cao YY, Lu CH et al (2015) A colorimetric assay for measuring iodide using Au@Ag core-shell nanoparticles coupled with Cu^{2+}. Anal Chim Acta 891:269–276. https://doi.org/10.1016/j.aca.2015.06.043
21. Napakporn P, Tewarak P, Thitikan S et al (2020) Colorimetric assay for determination of Cu (II) ions using l-cysteine functionalized silver nanoplates. Microchem J 158:105101. https://doi.org/10.1016/j.microc.2020.105101
22. Zhou HY, Zhang H, Peng LJ et al (2022) L-cysteine-regulated in situ formation of Prussian blue/Turnbull's blue nanoparticles as the colorimetric probe for the detection of copper ion. Arab J Chem 15:104000. https://doi.org/10.1016/j.arabjc.2022.104000
23. Liu P, Hao R, Sun W et al (2022) One-pot synthesis of copper nanocluster/Tb-MOF composites for the ratiometric fluorescence detection of Cu^{2+}. Luminescence 37:1793. https://doi.org/10.1002/bio.4359
24. Yi WS, Chia LL, Chin FW et al (2018) A novel fluorescence sensor for dual sensing of Hg^{2+} and Cu^{2+} ions. J Photoch Photobio A 353:19–25. https://doi.org/10.1016/j.jphotochem.2017.11.003
25. Zhang N, Dai DQ, Hu PW et al (2022) Dual-modal photoelectrochemical and visualized detection of copper ions. ACS Omega 7:5415–5420. https://doi.org/10.1021/acsomega.1c06673
26. Lu JH, Zhang X, Liu NK et al (2016) Electrochemical detection of Cu^{2+} using graphene–SnS nanocomposite modified electrode.

Electroanal Chem 769:21–27. https://doi.org/10.1016/j.jelechem.2016.03.009
27. Hsieh MY, Huang PJ (2022) Magnetic nanoprobes for rapid detection of copper ion in aqueous environment by surface-enhanced Raman spectroscopy. RSC Adv 12:921–928. https://doi.org/10.1039/D1RA07482B